Design of a Multi-mode UWB Antenna Using Characteristic Mode Analysis

Qianyun Zhang, Runbo Ma, Wei Su, and Yue Gao

***Abstract*—In this communication, a low-profile ultra-wide band (UWB) antenna is designed, fabricated and measured for TV white space devices (TVWSDs). Starting from a simple annular ring, the proposed design procedure is guided by the characteristic mode analysis (CMA). Firstly, a closed-form estimation to the resonant frequencies of the first two characteristic modes for the annular ring structure are provided. Then the annular ring is modified to introduce more characteristic modes resonating within the interested spectrum. To excite these modes and to achieve a wideband antenna covering the whole ultra-high frequency (UHF) TV spectrum, the feeding structure is also carefully designed and refined. Finally, a prototype is fabricated and measured to verify its UWB performance, and radiation patterns at different frequencies are presented to prove the switching of dominating resonating modes. The analyses and performance evaluation show that the proposed antenna is a strong contender to be used for TVWSDs. Furthermore, thanks to the simplicity of tuning and controlling modal resonant frequencies, this procedure can be flexibly applied to various antenna designs.**

***Index Terms*—Characteristic mode analysis, UHF, UWB antenna, TV white space**

I. Introduction

TV white space (TVWS) refers to the set of vacant frequency bands not occupied by the licensed broadcasting services and are available for unlicensed use. Due to the low operating frequency, devices working at TVWS benefit from low energy consumption and wide communication coverage. In 2008, the Federal Communications Commission (FCC) firstly approved unlicensed use of TVWS [1], and later the license-exempt use of TVWS was also enabled in the United Kingdom by the Office of Communications (Ofcom) [2]. Having good propagation property and being cost effective, the TVWS has attracted a lot of attention from regulators, academia, and industry to build connections among participants in M2M systems [3].

Since the operating frequencies of TVWS devices (TVWSDs) are dynamically obtained from geo-location database, spectrum sensing or their combination [4], antennas covering the entire TV spectrum is required for TVWSDs. FCC has defined a radio system an ultra-wide band (UWB) system if its fraction bandwidth is greater than 20% or the absolute bandwidth wider than 500 MHz [5]. In the United Kingdom, spectrum reserved for the digital terrestrial television services is from 470 MHz to 790 MHz over the ultra-high frequency (UHF) and the fractional bandwidth of the UHF TV spectrum exceeds 50%. In recent years, UWB antennas operating in the UHF band have been intensively studied [6]–[8]. In [6], the magneto-dielectric material was used to enhance the impedance bandwidth of a 3D inverted-F antenna. Next, by applying different bias voltages on an integrated varactor diode, the antenna operation frequency was tuned from 470 MHz to 862 MHz. However, the antenna efficiency was sacrificed because of the material loss and the tuning circuit. In [7] and [8], the entire UHF TV spectrum was covered by the combination of two resonances contributed by different radiating elements. However, no insight into the radiation properties of a single element was given in works above, which may lead to inflexible UWB antenna designs.

Acquiring full characteristics of a radiating body with arbitrary geometry, the characteristic mode analysis (CMA) provides a way to reveal physical essence of antennas [9]. In the last several decades since its inception, the CMA has been applied to various problems including antenna analysis, synthesis and optimization [10]–[13], and a comprehensive review of the state-of-the-art CMA applications in engineering can be found in [14]. In [11], potential of a TM10 antenna was investigated by examining different characteristic modes, and the antenna bandwidth was nearly doubled by combining multiple resonances. In [12], to overcome the difficulty of implementing low-coupling multi-antennas operating below 1 GHz in compact mobile handsets, multiple characteristic modes were created by manipulating the chassis structure, and the multi-antenna structure was realized by exciting these modes individually.

Following our preliminary work in [15], we consider creating multiple resonating modes using CMA to enhance the bandwidth. More specifically, in this communication the CMA is firstly performed on an annular ring to find a closed-form estimation calculating resonant frequencies of its two dominant modes, and then slots are cut to decrease the resonate frequencies. Next, multiple characteristic modes with resonant frequencies distributed over the spectrum of interest are created by manipulating the ring structure. After having sufficient characteristic modes, the feeding structure is designed to excite them efficiently. In this way, by exciting multiple characteristic modes, the proposed structure is optimized to cover the whole UHF TV spectrum. Finally, a prototype is fabricated and measured to verify simulation analyses and the measurement results show that the proposed antenna achieves 71% fractional bandwidth.

II. CMA on an annular ring and feeding design

Based on the theory of characteristic mode (TCM) [9], any structure is capable to support multiple characteristic modes with orthogonal characteristic currents ($\mathbf{J}_n$), and their corresponding eigenvalues (λ_n) are obtained from

$$\mathbf{X}(\mathbf{J}_n) = \lambda_n \mathbf{R}(\mathbf{J}_n), \tag{1}$$

where $\mathbf{X}$ and $\mathbf{R}$ are imaginary and real parts of the impedance matrix calculated by the method of moment. Eigenvalue represents the ratio between the energy stored near the structure ($P_{reac,n}$) and the radiated energy ($P_{rad,n}$) associated with the n^{th} mode [9],

$$\lambda_n = \frac{<\mathbf{J}_n^*, \mathbf{X}(\mathbf{J}_n)>}{<\mathbf{J}_n^*, \mathbf{R}(\mathbf{J}_n)>} = \frac{P_{reac,n}}{P_{rad,n}}, \tag{2}$$

in which $*$ is the conjugate operator. From (2), modes with $\lambda_n = 0$ are at resonance and all energy is radiated; $\lambda_n < 0$ means the stored energy is dominated by the electric energy, and the associated mode is a capacitive mode; on the contrary, mode with $\lambda_n > 0$ is an inductive mode. To simplify the identification of modal characteristics, the characteristic angle α_n is often used and it is defined as

$$\alpha_n = 180^o - tan^{-1}(\lambda_n). \tag{3}$$

The work was supported by Physical Sciences Research Council (EPSRC) in the U.K. under Grant EP/R00711X/1.

Qianyun Zhang, Wei Su and Yue Gao are with the School of Electronic Engineering and Computer Science, Queen Mary University of London, London E1 4NS, U.K. (emails: qianyun.zhang@qmul.ac.uk; w.su@qmul.ac.uk, yue.gao@qmul.ac.uk).

Runbo Ma is with College of Physics and Electronics Engineering, Shanxi University, Taiyuan 030006, China (email: marunbo@sxu.edu.cn)

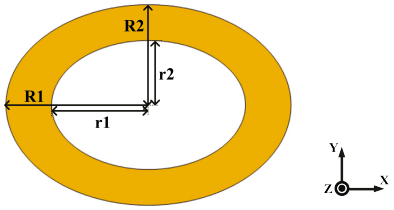

Fig. 1: Geometry of an annular ring (R_1=100 mm, R_2=70 mm, r_1=68 mm, and r_2=45 mm).

Thus, for an inductive mode $90^\circ < \alpha_n < 180^\circ$, and $180^\circ < \alpha_n < 270^\circ$ for a capacitive mode. Resonance occurs when $\alpha_n = 180^\circ$.

A. CMA on an Annular Ring

Before getting into details of the proposed antenna, we first perform the CMA on a metal annular ring which is the basic structure of the proposed antenna. For a ring depicted in Fig. 1, modal current distributions and radiation patterns of its first three modes are presented in Fig. 2. In this communication, modal current distributions and radiation patterns are given at resonant frequencies of the corresponding modes, which, according to Fig. 3, are 708 MHz for mode 1 and 794 MHz for mode 2. As shown in Figs. 2(a) and (b), the currents of mode 1 and mode 2 flow along the long and the short axes of the ring, respectively, and corresponding to their orthogonal current distributions, mode 1 has a donut-like radiation pattern with nulls at the x-axis, while nulls of the radiation pattern turn 90° to the y-axis for mode 2. The current of mode 3 flows as a closed loop, and thus it behaves inductively, which can also be verified from Fig. 3 where its characteristic angles are all below 180° over the entire simulated spectrum. Because mode 3 cannot resonate, its current distribution and radiation pattern at the centre frequency of the simulated band (i.e. 950 MHz) are given as illustrations, which also applies to Fig. 4(c) and Fig. 6(d).

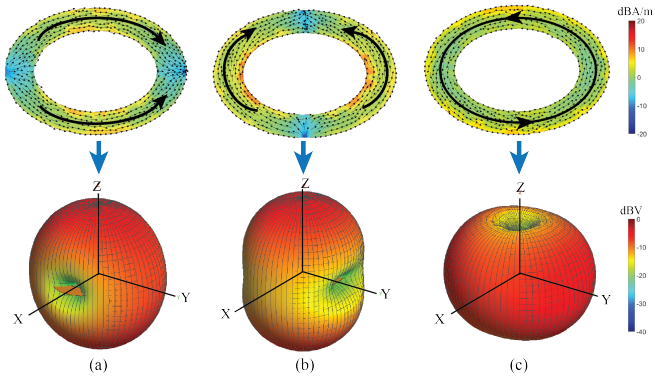

Fig. 2: Modal current distributions and radiation patterns of (a) mode 1 at 708 MHz, (b) mode 2 at 794 MHz, and (c) mode 3 at 950 MHz on the annular ring shown in Fig. 1.

As introduced above, mode 1 and mode 2 behave like half-wave resonators whose resonant frequencies are $c/4R$, where c is the speed of light in the vacuum and $2R$ is the effective electrical length. Using $R = R_1 = 100$ mm for mode 1 and $R = R_2 = 70$ mm for mode 2, the calculated resonant frequencies are 750 MHz and 1071 MHz for the two modes (resonating at 708 MHz and 794 MHz, respectively, in simulation). The significant difference between the estimated and simulated results is because the annular ring is elliptically shaped and the currents always concentrate near the edge,

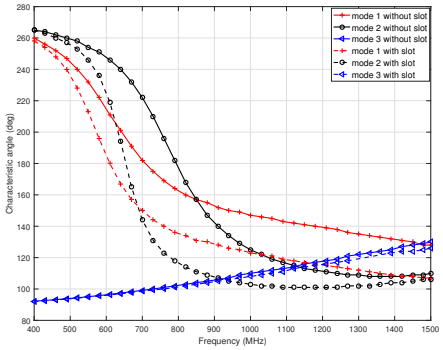

Fig. 3: Characteristic angles of modes 1-3 for annular rings with and without slots.

TABLE I: The polynomial coefficients of (4) calculating the resonant frequency (in MHz) of mode 1.

parameter	k = 0.3	k = 0.4	k = 0.5	k = 0.6	k =0.7
p_{00}	818.3	806.9	894.8	924.2	1008
p_{10}	-244.6	-202.8	-322.6	-303.6	-385.5
p_{01}	103.3	134.7	50.48	-18.61	-139.2
p_{20}	186.7	178.7	235.9	236.9	295.5
p_{11}	13.89	-30.38	31.39	13.81	23.06
p_{02}	-217.2	-250.9	-271.6	-254.4	-225

and thus the effective modal electrical lengths used for estimation are not accurate. Moreover, these lengths also vary with geometry parameters of annular rings. Therefore, to provide a general design reference for annular ring-shaped antennas, it is crucial to clarify the relationship between dimensions of the annular ring and resonant frequencies of the basic modes (mode 1 and mode 2). Fortunately, with the help of CMA, resonate frequencies of the two modes for structures with arbitrary dimensions can be found numerically.

For a given R_1, here we introduce another three parameters, the axis ratio of the outer ellipse $k = R_2/R_1$, the ratio of horizonal axes of the inner and the outer ellipse $k_1 = r_1/R_1$ and the ratio of their vertical axes $k_2 = r_2/R_2$ to determine dimensions of the annual ring structure. Then resonant frequency (in MHz) of mode 1 and mode 2 can be approximated by a polynomial of k_1 and k_2:

$$f(k_1, k_2) = p_{00} + p_{10}k_1 + p_{01}k_2 + p_{20}k_1^2 + p_{11}k_1k_2 + p_{02}k_2^2 \quad (4)$$

The polynomial coefficients deciding resonant frequencies of mode 1 and mode 2 for different k when $R_1 = 100$ mm are presented in TABLE I and TABLE II. For different R_1, the resonant frequencies can be obtained through the scaling relation. Since modal currents have strong intensities near the inner edge of the annular ring, as k_1 and k_2 decrease dramatically, the effective electrical length also decreases, and thus the corresponding resonant frequency increases rapidly. To persevere the accuracy of the polynomial fitting, k_1 and k_2 in (4) are confined to be larger than 0.3.

Based on the fitted polynomial above, with geometry parameters given in Fig. 1 (i.e. $k = 0.7$, $k_1 = 0.68$, and $k_2 = 0.64$), the estimated resonant frequencies are 710 MHz and 789 MHz for mode 1 and mode 2, which are quite close to the simulated results.

B. Cutting Slots on the Annular Ring

Cutting slots at locations with strong currents can significantly increase the effective modal electrical lengths and reduce modal resonant frequencies, while slots at locations with weak currents barely affect the resonances. Therefore, to reduce the resonant frequencies of mode 1 and mode 2, slots are cut on the ring where modal current

TABLE II: The polynomial coefficients of (4) calculating the resonant frequency (in MHz) of mode 2.

parameter	k = 0.3	k = 0.4	k = 0.5	k = 0.6	k =0.7
p_{00}	2929	2646	2580	2244	2001
p_{10}	-4020	-3325	-3299	-2570	-2135
p_{01}	-184	-396.6	-555.8	-525	-521.2
p_{20}	1855	1429	1463	1015	782.8
p_{11}	4.11	83.59	176.6	158.1	182.3
p_{02}	192.6	311.7	368.7	339.1	322.5

strengths are strong based on Figs. 2(a) and (b). After a thorough simulation study, we found that with dimensions of the annular ring fixed, at least three slots at each area with strong modal currents are needed to reach the lowest band of the desired frequency. The structure with slots is illustrated in Fig. 4 where updated modal current distributions and radiation patterns of the slotted annular ring are also provided.

Characteristic angles of modes 1-3 are simulated again for the slotted annular ring, and results are plotted in Fig. 3 together with those of the ring without slots. It is noticed that the resonant frequencies of modes 1 and 2 have reduced to 610 MHz and 654 MHz, respectively. The characteristic angle curve of mode 3 remains unchanged since the modal current flow is barely affected by the inserted slots, which can be seen from current distributions of Fig. 2(c) and Fig. 4(c). Moreover, according to radiation patterns given in Fig. 2 and Fig. 4, cutting slots on the ring has very slight effect on modal radiation patterns.

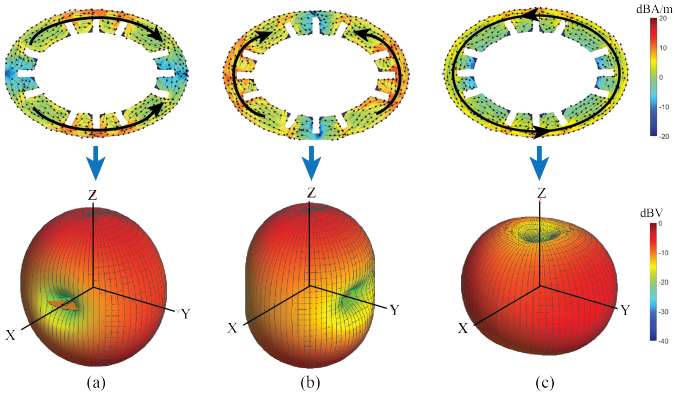

Fig. 4: Modal current distributions and radiation patterns of (a) mode 1 at 610 MHz, (b) mode 2 at 654 MHz, and (c) mode 3 at 950 MHz on the annular ring with slots.

C. CMA with Feeding Structure

A rectangular metal strip, which serves as the feeding structure, along the long axis of the annular ring is then placed 3.1 mm below the ring as shown in Fig. 5. Normally, new characteristic modes would be introduced after adding new components to the existing structure. Thus, CMA is performed on the new whole structure whose modal currents and radiation patterns are illustrated in Fig. 6.

For this new structure, we name modes having currents along the long axis of the ring, illustrated in Figs. 6(a) and (b), as mode 1^a and mode 1^b, since they exhibit similar radiation behavior as that of mode 1 given in Fig. 2(a). The difference between these two modes is that currents on the rectangular strip and the annular ring have opposite directions for mode 1^a, while their directions are the same for mode 1^b. Radiation patterns and current distributions on the ring

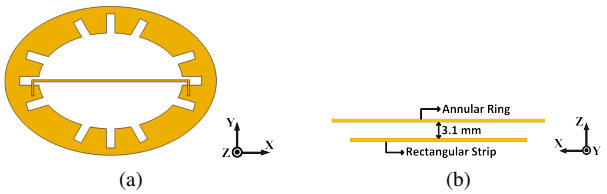

Fig. 5: Structure layout of the slotted annular ring with a rectangular strip (a) top view and (b) side view.

structure in Figs. 6(c) and (d) are almost identical to those without a strip, and thus we still name them as mode 2 and mode 3.

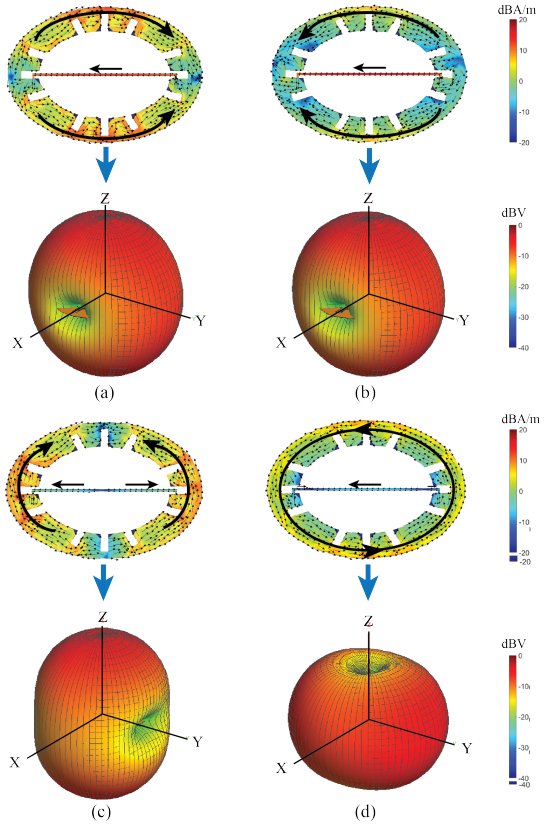

Fig. 6: Modal current distributions and radiation patterns of (a) mode 1^a at 553 MHz, (b) mode 1^b at 809 MHz, (c) mode 2 at 654 MHz, and (d) mode 3 at 950 MHz on the structure containing a ring and a rectangular strip.

Characteristic angles of mode 1^a, mode 1^b, mode 2, and mode 3 are presented in Fig. 7(a). From these characteristic angle curves, mode 1^a resonates at 553 MHz, while mode 1^b resonates at 809 MHz. The resonant frequency of mode 2 is 654 MHz, and characteristic angles of mode 3 are still below 180° over the simulated spectrum.

When the radiating body is excited, the resultant current $\mathbf{J}$ on the structure can be decomposed into a linear combination of modal currents

$$\mathbf{J} = \sum w_n \mathbf{J}_n, \tag{5}$$

where w_n is the weight coefficient of the n^{th} mode and it is calculated by

$$w_n = \frac{\iint \mathbf{J}_n^* \cdot E_{in} dS}{1 + j\lambda_n}, \tag{6}$$

in which E_{in} is the current produced by the excitation source on the port.

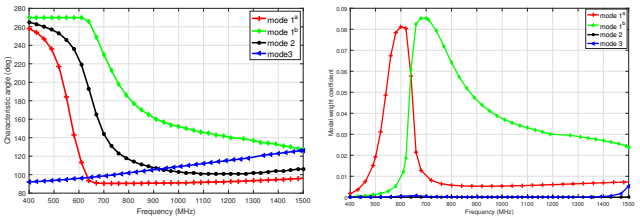

(a) (b)

Fig. 7: (a) Characteristic angels and (b) modal weight coefficients of modes 1^a, 1^b, 2, and 3 given in Fig. 6.

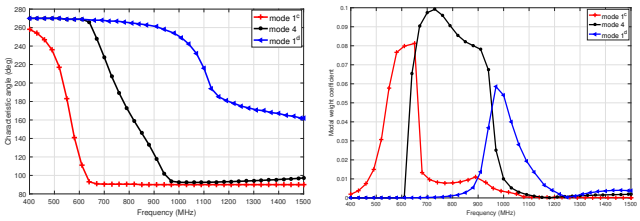

(a) (b)

Fig. 9: (a) Characteristic angels and (b) modal weight coefficients of modes 1^c, 4, and 1^d given in Fig. 8.

Applying a delta-gap source at the middle of the strip, the rectangular strip operates as a dipole, and its radiated electromagnetic energy will be coupled to the annular ring and produce induced current, and therefore the ring structure is excited. The modal weight coefficients of mode 1^a, mode 1^b, mode 2, and mode 3 are obtained and shown in Fig. 7(b). As we can see from this figure, only two modes (mode 1^a and mode 1^b) are significantly excited. Apparently, these two modes are not sufficient to cover the entire UHF TV spectrum, and hence more characteristic modes resonating in the UHF band are required to satisfy the UWB requirement.

Based on analyses above, in this communication, we would like to utilize variations of mode 1 and mode 2 to contribute to the total radiation. Since mode 2 behaves similar to mode 1 but with current along an orthogonal direction, mode 1 and its variations are discussed next in detail.

III. Structure Modification and Feeding Refinement

A. Structure Modification

Since the resonant frequencies of modes 1^a and 1^b are 553 MHz and 810 MHz, respectively, to achieve a fractional bandwidth over 50% as required by the TV frequency band, a higher resonance at around 1200 MHz is expected. Therefore, a smaller ring is inserted into the original one as shown in Fig. 8 to generate more characteristic modes. Choosing $R_1 = 50$ mm and $k = 0.6$, when $k_1 = 0.6$ and $k_2 = 0.83$ (i.e. $r_1 = 30$ mm and $r_2 = 25$ mm), the resonant frequency of mode 1 is 1287 MHz based on (4). In addition, the final resonant frequency might be smaller than the estimation because of the capacitance between feeding dipoles and rings.

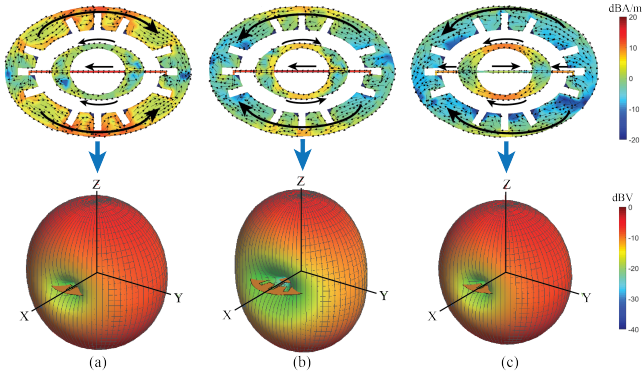

Fig. 8: Modal current distributions and radiation patterns of (a) mode 1^c at 552 MHz, (b) mode 4 at 776 MHz, and (c) mode 1^d at 1198 MHz on the structure containing double rings and a rectangular strip.

CMA simulation is then performed on the structure with double rings and modes with currents along the long axis of the ring are given in Figs. 8(a), (b), and (c), which are named as mode 1^c, mode 4, and mode 1^d, respectively. All the three modes can be regarded as variations of mode 1 owing to similar radiation patterns with that of mode 1, and their characteristic angles are presented in Fig. 9(a). From Fig. 7(a) and Fig. 9(a), the characteristic angle curve of mode 1^c overlaps with that of mode 1^a, which is reasonable because the two modes have almost identical current distributions on the outer ring, and the current of mode 1^c is weak on the inner ring. The reason we name the mode with current distribution shown in Fig. 8(b) as mode 4 is that its currents on the outer and inner rings have close strengths but opposite directions, and more importantly, this is a new mode whose property is contributed by both the two rings. Based on Fig. 8(c), mode 1^d is mainly determined by the inner ring and it resonates at 1198 MHz, which is close to the estimation before.

Using the thin strip as a driven element, the modal weight coefficients of modes 1^c, 4, and 1^d are plotted at Fig. 9(b). It can be seen that weights of mode 1^c and mode 4 are high at frequencies close to their resonances, which indicates that they are properly excited. Comparing Fig. 7(b) and Fig. 9(b), it is observed that adding an inner ring not only creates higher resonances, but also achieves high modal weight coefficients over wider band. However, although the design at this stage has the potential to realize a good radiation from 1200 MHz to 1500 MHz due to the existence of mode 1^d, the long strip cannot excite this mode efficiently.

B. Feeding Refinement

To excite mode 1^d and to improve the antenna performance at high frequency band, a shorter strip is added to the original feeding structure as illustrated in Fig. 10. With the additional strip, characteristic angles and modal weight coefficients of mode 1^c, 4, and 1^d are presented in Figs. 11(a) and (b). Comparing results in Fig. 11(a) and Fig. 9(a), it is noticed that adding a shorter strip has little effect to mode 1^c and mode 4, while characteristic angles of mode 1^d becomes less flat near its resonance. Nevertheless, after the feeding structure refinement, weights of mode 1^d near its resonance are higher as shown in Fig. 11(b).

(a) (b)

Fig. 10: Structure layout of double rings with two rectangular strips (a) top view and (b) side view.

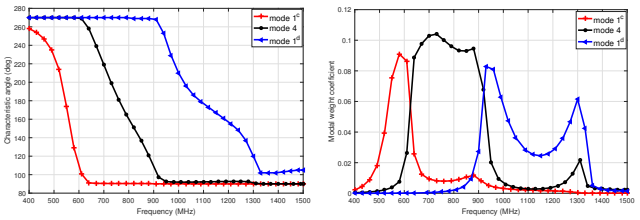

(a) (b)

Fig. 11: (a) Characteristic angles and (b) modal weight coefficients of modes 1^c, 4, and 1^d corresponding to structure shown in Fig. 10.

IV. Antenna Optimization and Measurement

A. Antenna Optimization

After exciting all the expected modes having currents along the long axis of the ring, two dipoles along the short axis are used to excite variations of mode 2, and characteristic modes of the whole structure are analyzed. As shown in Figs. 12(a) and (b), mode 2^c corresponds to mode 1^c, whose radiation mainly depends on the outer ring, but currents of mode 2^c are along the short axis of the ring. Similarly, mode 5 and mode 2^d are corresponding to mode 4 and

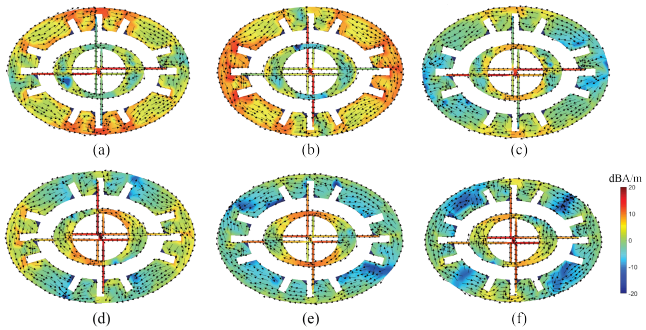

Fig. 12: Modal current distributions on the structure containing two rings and four strips (a) mode 1^c at 546 MHz, (b) mode 2^c at 581 MHz, (c) mode 4 at 760 MHz, (d) mode 5 at 981 MHz, (e) mode 1^d at 1102 MHz, and (f) mode 2^d at 1500 MHz.

mode 1^d, respectively. However, for mode 5, when the longer vertical strip is in operation, the shorter horizontal strip begins to work with the increase of frequency, and hence positions of current nulls are rotated. Operation of strips orthogonal to the original modal current directions also make current nulls of modes 1^d and 2^d rotate. It is worth mentioning that mode 2^d has not resonated over the simulated frequency band according to Fig. 13(a), so its current distribution is given at 1500 MHz where the characteristic angle is the closest to 180°.

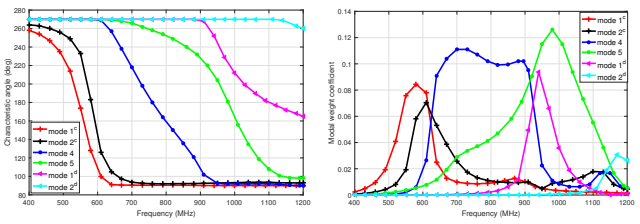

(a) (b)

Fig. 13: (a) Characteristic angles and (b) modal weight coefficients of modes 1^c, 2^c, 4, 5, 1^d, and 2^d given in Fig. 12.

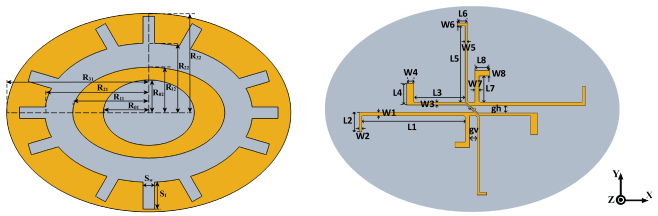

(a) (b)

Fig. 14: Structure layout of the final antenna (a) top view and (b) bottom view.

TABLE III: Dimensions of the proposed antenna

Parameter	R_{01}	R_{02}	R_{11}	R_{12}	R_{21}	R_{22}	R_{31}
Value (mm)	30.9	21.5	55.1	31.2	73.0	49.0	100.0
Parameter	R_{32}	S_I	S_w	gh	gv	L1	W1
Value (mm)	70.0	19.1	8.0	4.6	5.6	69.9	2.2
Parameter	L2	W2	L3	W3	L4	W4	L5
Value (mm)	14.5	1.9	36.0	2.1	13.4	5.0	51.3
Parameter	W5	L6	W6	L7	W7	L8	W8
Value (mm)	1.8	6.2	1.9	18.0	2.8	9.9	3.9

Characteristic angles and modal weight coefficients of modes 1^c, 2^c, 4, 5, 1^d, and 2^d are given in Fig. 13. According to Fig. 13(a), resonant frequencies of modes 1^c, 2^c, 4, 5, and 1^d are 546 MHz, 581 MHz, 760 MHz, 981 MHz, and 1102 MHz, respectively. In addition, modal weight coefficients shown in Fig. 13(b) indicate that the 5 modes contribute to the final radiation in turn.

As shown in Fig. 14, the structure is then printed on a 3.1 mm-thick Rogers5880 PCB board for easier fabrication and further operating frequency reduction. The proposed structure, which has also been presented in [15] but without systematic CMA, is further simulated and optimized in the CST Microwave Studio with substrate included, and the final dimensions are summarized in TABLE III.

B. Antenna Measurement

An antenna prototype is then fabricated and measured in Queen Mary University of London. Photos of the antenna are shown in Fig. 15. The simulated and measured reflection coefficients are given in Fig. 16(a), according to which, the proposed antenna achieves -10 dB impedance bandwidth from 470-987 MHz in measurement, and the simulated operation spectrum is from 470 MHz to 951 MHz. Fig. 16(b) gives the peak realized gain for the proposed antenna over 470-1000 MHz. It is observed that the measured gain is between 2.5 dBi and 3.8 dBi over the UWB operation frequency. The measurement results agree well with those in simulation, and small differences might be introduced from measurement environment and fabrication imperfections.

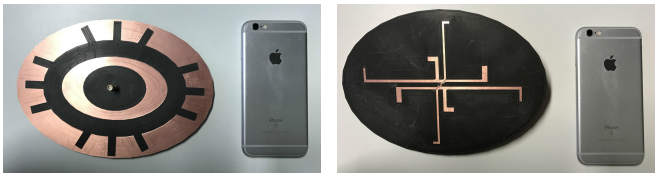

(a) (b)

Fig. 15: Prototype of the proposed antenna (a) top view and (b) bottom view.

The simulated and measured radiation patterns at 500 MHz, 600 MHz, 700 MHz, and 800 MHz in the XZ and YZ planes are shown in Fig. 17. Effects of cables and unavoidable scattering in the

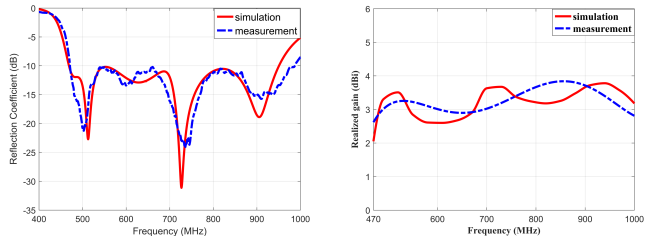

(a) (b)

Fig. 16: (a) Simulated and measured reflection coefficients and (b) realized gain of the proposed antenna.

chamber could be the source of discrepancies between measurement and simulation results. It is observed that the relative magnitudes of E_θ and E_ϕ vary with frequency, which is because multiple modes having orthogonal polarization directions are excited to different extents and the dominant resonant mode changes over the operating band. In practical, due to the random device directivities and the multipath effects resulted from complex M2M communication environment, signals have random polarization directions and a near-omnidirectional radiation pattern is advantageous [16], [17]. Moreover, we have to note that there is no special balun structure used to eliminate possible effects from the unbalanced coaxial cable. This is because the proposed planar antenna is directly integrated on TVWSDs and the leaky current on the outer surface of the electrically short coaxial connector barely affects the final performance of the proposed antenna over its operating frequency band.

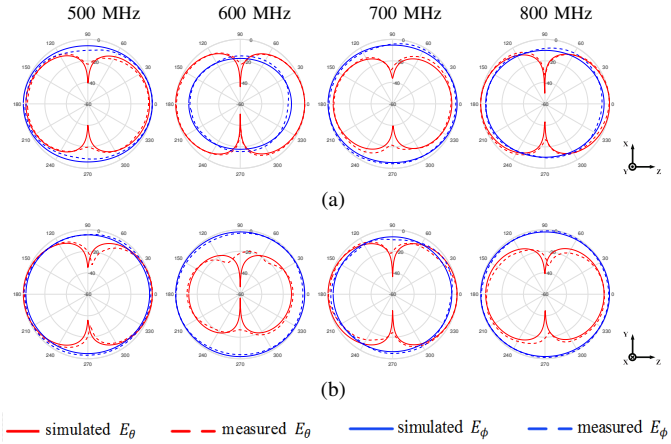

Fig. 17: Simulated and measured radiation patterns in the (a) XZ plane and (b) YZ plane.

V. Conclusion

This communication presents a design procedure of a UWB antenna operating over the entire UHF TV spectrum for TVWSDs. Starting from a simple annular ring structure, the CMA is used as a powerful tool to provide insights into generating and exciting multiple modes to achieve wideband performance. Based on current distributions of the desired characteristic modes on the annular ring, slots are cut on the structure to decrease modal resonant frequencies. In addition, by inserting a smaller ring into the original one, more characteristic modes resonating in the interested frequency band are generated and the UWB property is established. By observing properties of each mode, the feeding structure is designed to excite all the desired modes efficiently, and the UWB performance is finally achieved through combining resonances of multiple modes. Although the final antenna structure is complicated, the design methodology and the functionality of each component are clear. Furthermore, the resonant frequency of each characteristic mode can be tuned by changing dimensions of the two rings, and the modes can be excited selectively. Therefore, our design procedure for UWB antenna using CMA could be flexibly applied to satisfy various antenna design requirements. For example, by tuning modal resonances to widely separated frequencies, multi-band antennas could be achieved.

References

[1] Federal Communications Commission (FCC). (2010, Sep.). *In the Matter of Unlicensed Operation in the TV Broadcast Bands, Additional Spectrum for Unlicensed Devices Below 900 MHz and in the 3 GHz Band, Second Memorandum Opinion and Order*. [Online]. Available: http://www.adaptrum.com/docs/FCC-10-174A1.pdf

[2] U.K. Office of Communications (Ofcom). (2012, Nov.). *TV white spaces-A consultation on white space device requirements*. [Online]. Available: http://stakeholders.ofcom.org.uk/binaries/consultations/whitespaces/summary/condoc.pdf

[3] M. Dohler and Y. Gao, "Spectrum to unlash machine-to-machine uptake," *Opportunistic Spectrum Sharing and White Space Access: The Practical Reality*, pp. 649–677, 2015.

[4] Z. Qing, Y. Gao, and C. G. Parini, "Data-assisted low complexity compres- sive spectrum sensing on real-time signals under sub-nyquist rate," *IEEE Trans. Wireless Commun.*, vol. 15, no. 2, pp. 1174–1185, Feb. 2016.

[5] FCC, "First report and order in the matter of revision of part 15 of the commission's rules regarding ultra-wideband transmission systems. et-docket. 2002: 98-153," Apr. 2002.

[6] L. Huitema, T. Reveyrand, J. L. Mattei, E. Arnaud, C. Decroze, and T. Monediere, "Frequency tunable antenna using a magneto-dielectric material for dvb-h application," *IEEE Trans. Antennas Propag.*, vol. 61, no. 9, pp. 4456–4466, 2013.

[7] Y. W. Chi, K. L. Wong, and S. W. Su, "Broadband printed dipole antenna with a step-shaped feed gap for dtv signal reception," *IEEE Trans. Antennas Propag.*, vol. 55, no. 11, pp. 3353–3356, 2007.

[8] R. Caso, A. D'Alessandro, A. A. Serra, P. Nepa, and G. Manara, "A compact dual-band pifa for dvb-t and wlan applications," *IEEE Trans. Antennas Propag.*, vol. 60, no. 4, pp. 2084–2087, 2012.

[9] R. F. Harrington and J. R. Mautz, "The theory of characteristic modes for conducting bodies," *IEEE Trans. Antennas Propag.*, vol. 19, no. 5, pp. 622–628, May 1971.

[10] Y. Chen and C. F. Wang, "Electrically small uav antenna design using characteristic modes," *IEEE Trans. Antennas Propag.*, vol. 62, no. 2, pp. 535–545, 2014.

[11] J. J. Adams and J. T. Bernhard, "A modal approach to tuning and bandwidth enhancement of an electrically small antenna," *IEEE Trans. Antennas Propag.*, vol. 59, no. 4, pp. 1085–1092, 2011.

[12] H. Li, Z. T. Miers, and B. K. Lau, "Design of orthogonal mimo handset antennas based on characteristic mode manipulation at frequency bands below 1 ghz," *IEEE Trans. Antennas Propag.*, vol. 62, no. 5, pp. 2756–2766, 2014.

[13] K. K. Kishor and S. V. Hum, "A pattern reconfigurable chassis-mode mimo antenna," *IEEE Trans. Antennas Propag.*, vol. 62, no. 6, pp. 3290–3298, 2014.

[14] Y. Chen and C. F. Wang, *Characteristic modes: Theory and applications in antenna engineering*. John Wiley & Sons, 2015.

[15] Q. Zhang and Y. Gao, "Design of an uhf uwb doubled annular ring antenna using characteristic mode analysis," in *2017 IEEE* 11^{th} *European Conference on Antennas and Propagation (EUCAP)*, pp. 3464–3466.

[16] Q. Zhang, X. Zhang, O. Holland, M. Dohler, J. M. Chareau, Y. Gao, and P. Chawdhry, "Tv white space network provisioning with directional and omni-directional terminal antennas," in *2016 IEEE* 84^{th} *Vehicular Technology Conference (VTC-Fall)*, pp. 1–5.

[17] K. L. Wong and M. T. Chen, "Small-size lte/wwan printed loop antenna with an inductively coupled branch strip for bandwidth enhancement in the tablet computer," *IEEE Trans. Antennas Propag.*, vol. 61, no. 12, pp. 6144–6151, 2013.